Different Structural Changes Occur in Blue- and Green-Proteorhodopsins during the Primary Photoreaction†

Jason J. Amsden,‡ Joel M. Kralj,‡ Vladislav B. Bergo,‡,§ Elena N. Spudich,§ John L. Spudich,§ and Kenneth J. Rothschild*,‡

Department of Physics, Photonics Center, and Molecular Biophysics Laboratory, Boston University, Boston, Massachusetts 02215, and Center for Membrane Biology, Department of Biochemistry and Molecular Biology, University of Texas Medical School, Houston, Texas 77030

Received May 20, 2008; Revised Manuscript Received August 28, 2008

ABSTRACT: We examine the structural changes during the primary photoreaction in blue-absorbing proteorhodopsin (BPR), a light-driven retinylidene proton pump, using low-temperature FTIR difference spectroscopy. Comparison of the light-induced BPR difference spectrum recorded at 80 K to that of green-absorbing proteorhodopsin (GPR) reveals that there are several differences in the BPR and GPR primary photoreactions despite the similar structure of the retinal chromophore and all-*trans* → 13-*cis* isomerization. Strong bands near 1700 cm^{-1} assigned previously to a change in hydrogen bonding of Asn230 in GPR are still present in BPR. However, additional bands in the same region are assigned on the basis of site-directed mutagenesis to changes occurring in Gln105. In the amide II region, bands are assigned on the basis of total ^{15}N labeling to structural changes of the protein backbone, although no such bands were previously observed for GPR. A band at 3642 cm^{-1} in BPR, assigned to the OH stretching mode of a water molecule on the basis of $H_2{}^{18}O$ substitution, appears at a different frequency than a band at 3626 cm^{-1} previously assigned to a water molecule in GPR. However, the substitution of Gln105 for Leu105 in BPR leads to the appearance of both bands at 3642 and 3626 cm^{-1}, indicating the waters assigned in BPR and GPR exist in separate distinct locations and can coexist in the GPR-like Q105L mutant of BPR. These results indicate that there exist significant differences in the conformational changes occurring in these two types proteorhodopsin during the initial photoreaction despite their similar chromophore structures, which might reflect a different arrangement of water in the active site as well as substitution of a hydrophilic for hydrophobic residue at residue 105.

Proteorhodopsins (PRs)[1] are members of the microbial rhodopsin family. Since their initial discovery in Monterey Bay (*1*), over 4000 different variants have been discovered using environmental genome sequencing techniques (*2*−*4*). It is estimated that PR-containing bacteria account for 13% of the microorganism species in the ocean photic zone (*5*). The widespread distribution of PR in worldwide oceanic waters indicates that PR phototrophy is a significant oceanic microbial process (*5, 6*).

Similar to BR and other microbial rhodopsins, PRs consist of seven transmembrane α-helices containing a retinylidene chromophore covalently bound to a lysine (Lys231) via a protonated Schiff base (*1*). Light absorption by PR results in an all-*trans* to 13-*cis* isomerization of the retinal which then drives a series of reaction steps that result in a proton being pumped from the cytoplasm to the extracellular medium (*7, 8*).

There are two major subgroups of proteorhodopsins characterized by their visible absorption maxima. The green-absorbing proteorhodopsin (GPR) subgroup absorbs maximally at ∼520 nm and functions as a light-driven proton pump similar to bacteriorhodopsin (BR) (*1, 7*−*9*). A second subgroup called blue-absorbing proteorhodopsin (BPR) absorbs near 490 nm (*6*). The different variants of PRs are thought to have evolved through Darwinian selection (*10*). One difference between GPR and BPR which was found to be a key determinant of their different properties is the identity of residue 105. (The numbering scheme for BPR is offset by one from GPR due to an extra glycine at residue 2 in BPR. Throughout, when referring to the amino acid positions in proteorhodopsins, the GPR numbering system is used.) In GPR residue 105 is a leucine while in BPR it is a glutamine (*11*−*14*). In a related paper, we show using resonance Raman spectroscopy that this residue is involved in tuning the visible absorption via interaction with the Schiff base and the C13 methyl of the retinal chromophore (*15*). BPR also pumps protons; however, it has a 10-fold slower photocycle than GPR. It has been suggested that the slower photocycle may indicate that BPR functions primarily as a

† This work was supported by National Institutes of Health Grants R01GM069969 (to K.J.R.) and R37GM27750 (to J.L.S.), Department of Energy Grant DE-FG02-07ER15867, and the Robert A. Welch Foundation (to J.L.S.).

* Corresponding author. E-mail: kjr@bu.edu. Phone: (617) 353-2603. Fax: (617) 353-9393.

‡ Boston University.

§ University of Texas Medical School.

[1] Abbreviations: BPR, blue-absorbing proteorhodopsin; GPR, green-absorbing proteorhodopsin; PR, proteorhodopsin; BR, bacteriorhodopsin; FTIR, Fourier transform infrared; C15D, retinal with a deuterium on carbon 15; OG, octyl glucoside; RRS, resonance Raman spectroscopy; HOOP, hydrogen out of plane; SRII, sensory rhodopsin II.

10.1021/bi800945t CCC: $40.75
Published on Web 10/09/2008

photoregulator rather than an energy harvesting pigment (*14, 16, 17*).

Fourier transform infrared (FTIR) difference spectroscopy has been successfully used to elucidate many of the details of the proton transport mechanism in BR (*18*−*21*) and GPR (*7, 8, 22*−*26*) as well to characterize the mechanisms of a variety of other microbial rhodopsins (*27, 28*). This study examines the initial events in the photocycle of BPR using static low-temperature FITR difference spectroscopy. The 80 K light-induced difference spectra reflect the formation of a red-shifted K-like photoproduct similar to the K-intermediates in GPR and light-adapted BR. Furthermore, the C═C and C−C retinal chromophore ethylenic and fingerprint stretching modes show that the primary photoreaction involves an all-*trans* → 13-*cis* isomerization of the retinal chromophore, although the difference spectrum also may exhibit small contributions from a 13-*cis* photocycle. Several prominent bands near 1700 cm^{-1} are assigned to structural changes of Asn230 and Gln105 side chains on the basis of site-directed mutations, indicating that these residues are perturbed in the earliest events of the BPR photocycle. In addition, a pair of bands at 1551 (−) and 1537 (+) cm^{-1} are assigned to an amide II downshift on the basis of total ^{15}N isotope labeling. Evidence is presented on the basis of assignment of bands to water molecule vibrations with $H_2{}^{18}O$ that there are two different sites for water molecules near the active site in BPR and GPR, respectively. In the Q105L mutant of BPR, which has a GPR-like visible absorption spectrum, both waters are present.

MATERIALS AND METHODS

Protein Expression and Purification. All procedures for the site-directed mutagenesis, plasmid construction, and expression in the *Escherichia coli* UT5600 strain were identical to those described previously (*14, 22*). *E. coli* cells containing the BPR WT or mutant-encoding plasmid (Hawaiian Ocean Time Station variant HOT75m4) or GPR WT-encoding plasmid (Monterey Bay strain eBAC 31A8) were cultured on standard Luria broth medium (Sigma Aldrich) and supplied with either all-*trans*-retinal or all-*trans*-retinal containing a deuterium on carbon 15 (C15D). Total ^{15}N labeling was achieved by growing *E. coli* containing the BPR-encoding plasmid on isotopically labeled growth media (Bioexpress cell growth media, U-15N, 98%; Cambridge Isotope Laboratories, Inc.). After the induction period, the cells expressing His-tagged wild-type or mutant BPR were centrifuged at 1000*g*, resuspended in 5 mM $MgCl_2$ and 150 mM Tris-HCl, pH 7.0, incubated with 100 μg/mL lysozyme for 2 h at 4 °C, and disrupted by sonication. Unbroken cells were removed by low-speed centrifugation. The membranes containing pigment were collected by centrifugation (39000*g*, 30 min) and solubilized in a wash buffer (50 mM potassium phosphate, 300 mM NaCl, 5 mM imidazole, and 1.5% octyl glucoside (OG), pH 7.0) for at least 1 h at 4 °C. Unsolubilized membranes were removed by centrifugation at 28000*g* for 30 min. The supernatant was incubated with a His-binding resin on a shaker at 4 °C for at least 1 h. The bound resin was applied to a 10 cm chromatography column and washed with 3× volume of wash buffer followed by elution buffer (50 mM potassium phosphate, 300 mM NaCl, 250 mM imidazole, and 1.0% OG, pH 7.0). The sample purity was assessed by UV−visible spectroscopy and SDS−PAGE analysis (*1*).

Proteoliposome Reconstitution. Purified His-tagged BPR was reconstituted in *E. coli* polar lipids (Avanti, Alabaster, AL) at 1:10 protein-to-lipid (w/w) ratio. Lipids initially dissolved in chloroform were dried under argon and resuspended in the dialysis buffer (50 mM potassium phosphate and 300 mM NaCl, pH 7.0) to which OG was added to the final concentration of 1%. The lipid solution was incubated with the OG-solubilized protein for 1 h on ice and dialyzed against the dialysis buffer with three buffer changes every 24 h. The reconstituted protein was centrifuged for 15 min and resuspended in the sample buffer (50 mM CHES and 150 mM NaCl, pH 9.5).

FTIR Difference Spectroscopy. The protein samples for the low-temperature FTIR measurements were prepared as previously reported (*22*−*24*) using approximately 200 μg of the protein for each experiment. The samples were deposited on CaF_2 windows and dried under a slow stream of argon. Samples were then rehydrated via the vapor phase and sealed in a sample cell with another CaF_2 window and mounted on a liquid nitrogen cryostat (ARS Cryo Helitran LT-3). Low-temperature FTIR difference spectra were recorded using a protocol similar to low-temperature FTIR difference measurements reported previously on GPR (*22*−*24*), BR (*19, 29*), and other microbial rhodopsins (*27, 28*). The BPR samples were first cooled to 80 K in the dark. They were then illuminated with blue light (415 nm < λ < 500 nm) for 5 min, and a spectrum of 1000 scans was recorded at 2 cm^{-1} after illumination using a Bio-Rad FTS-60A FTIR spectrometer (Bio-Rad, Digilab Division, Cambridge, MA) equipped with a liquid nitrogen cooled HgCdTe detector. The sample was then illuminated with long-wavelength orange light (800 nm > λ > 570 nm) for 5 min; a second spectrum was recorded in the dark after illumination and subtracted from the first. At least 24 such cycles of blue and orange light were repeated and the difference spectra averaged in order to increase the signal-to-noise ratio. In addition, all experiments were performed with at least two independent sample preparations to ensure reproducibility of the difference spectra. A Dolan-Jenner (Woburn, MA) model 180 illuminator (150 W, tungsten−halogen) and a fiberoptic light guide were used for sample illumination in combination with 500 nm low-pass and 570 nm long-pass optical filters (Corion Corp., Holliston, MA).

RESULTS

BPR Chromophore Normal Modes. The BPR 80 K light-induced difference spectrum (Figure 1) closely resembles a single "first push" difference spectrum, where spectra were measured before and after only the first blue light illumination (data not shown). This indicates that, like BR (*19, 29*), GPR (*22*−*24*), many other microbial rhodopsins (*27, 28*), and vertebrate rhodopsins (*30*), blue light converts the initial resting state of BPR to a K-like red-shifted photointermediate, while orange light photoreverses the reaction.

Similar to GPR (*8, 22*), BPR does not exhibit light−dark adaptation. For example, FTIR difference peaks are not observed above S/N (data not shown) upon recording a spectrum of a dark-adapted sample (i.e., the sample in the dark overnight at room temperature) and then subtracting

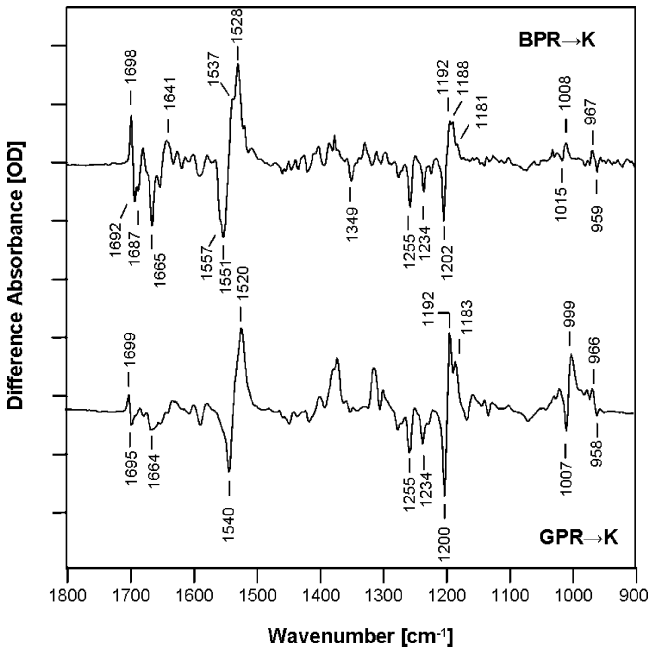

FIGURE 1: Comparison of FTIR difference spectra recorded at 80 K for BPR (top) and GPR (bottom) in the 900−1800 cm^{-1} spectral region. The spectra were recorded at 2 cm^{-1} spectral resolution. Each spectrum represents the average of at least 24 difference spectra, each consisting of 1000 individual scans. Spacing of *Y*-axis (difference absorbance) markers corresponds to 0.5 × 10^{-4} OD. Only the frequencies of bands discussed in paper in this and subsequent figures are labeled.

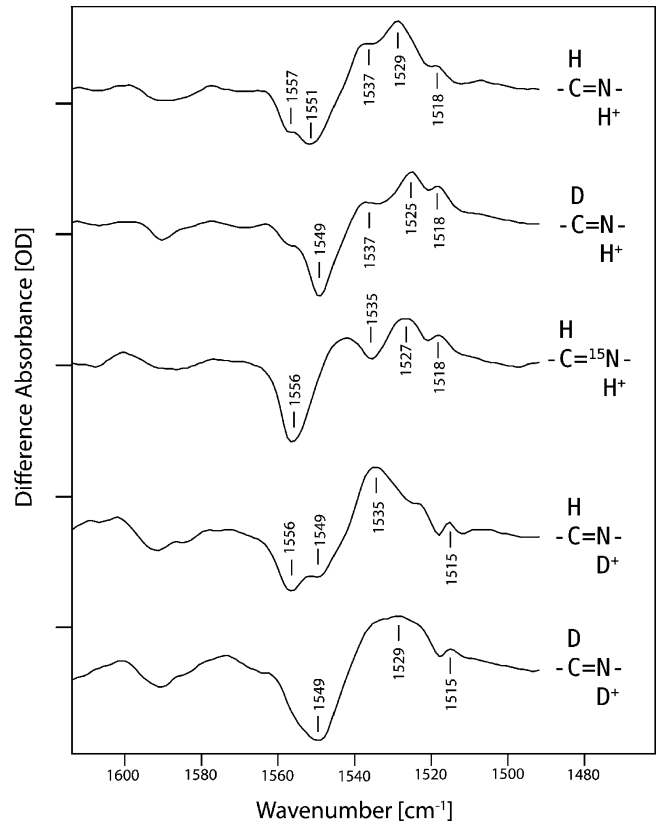

FIGURE 2: FTIR difference spectra recorded at 80 K and 2 cm^{-1} resolution for wild-type BPR containing unlabeled chromophore in H_2O, C15D-labeled chromophore in H_2O, unlabeled chromophore with total ^{15}N-labeled protein, unlabeled chromophore in D_2O, and C15D-labeled chromophore in D_2O. Spacing of *Y*-axis (difference absorbance) markers corresponds to 0.2 × 10^{-4} OD.

from it a spectrum recorded immediately after 5 min of illumination with >420 nm light. In addition, illuminating the sample prior to cooling to 80 K does not change the resulting BPR → K spectrum in contrast to a similar measurement for BR, which exhibits light−dark adaptation (*31*).

The FTIR difference spectrum of the BPR → K transition (Figure 1) shows that, like GPR and BR, the initial photochemistry involves all-*trans* to 13-*cis* isomerization of the retinylidene chromophore. In agreement, recent resonance Raman (RRS) measurements of BPR indicate that its chromophore has an all-*trans* structure very similar to GPR (*15*). In the ethylenic stretching region, there is a pair of negative bands at 1551 and 1557 cm^{-1} and a pair of positive bands at 1537 and 1529 cm^{-1} which could arise from the ethylenic stretching vibration of the initial state and photointermediate. The amide II normal mode of the peptide backbone could contribute to this region as shown recently in the subpicosecond IR difference spectrum of GPR at room temperature (*32*). To distinguish between these possibilities, we labeled the retinal with a deuterium on carbon 15 (C15D) which shifts the ethylenic frequency ∼5 cm^{-1} (*33*) and separately grew the protein on total ^{15}N-labeled media which shifts the amide II mode ∼15 cm^{-1} (*32, 34, 35*). As shown in Figure 2, in BPR regenerated with C15D retinal, the negative band at 1557 cm^{-1} downshifts to 1549 cm^{-1} while the positive band at 1529 cm^{-1} downshifts to 1525 cm^{-1}. Similarly, in a BPR sample which has undergone H/D exchange, bands at 1556 (−) and 1535 (+) cm^{-1} downshift to 1549 (−) and 1529 (+) cm^{-1} (Figure 2) with C15D-labeled retinal. Therefore, the 1557 (−) and 1529 (+) cm^{-1} bands are assigned to the ethylenic C═C stretching modes of the retinal chromophore in the initial and K-like photointermediates, respectively, similar to difference bands found in the GPR → K (*22*−*24*) and BR → K (*19, 29, 36, 37*) low-temperature FTIR difference spectra.

An empirical inverse relationship between the visible absorption maximum and the ethylenic stretching frequency has been established for rhodopsin (*38*) and microbial rhodopsins (see, for example, refs *22*, *27*, and *39*). This correlation predicts an approximately 5 nm red shift in λ_{max} for each 1 cm^{-1} decrease of the C═C stretching frequency. The 28 cm^{-1} downshift between the unphotolyzed state of wild-type BPR is larger than that of GPR (20 cm^{-1}) (*22*−*24*) and BR (15 cm^{-1}) (*19, 29, 36*). This indicates that BPR with a λ_{max} near 490 nm and its photointermediate may have a red shift in the visible absorption larger than the 60 nm spectral shift observed between BR_{570} and K_{630} at low temperature.

In BPR grown on total ^{15}N-labeled media (Figure 2), the ethylenic C═C band near 1556 cm^{-1} is unshifted while a band 1551 cm^{-1} band downshifts 16 cm^{-1} to 1535 cm^{-1}. The positive band at 1537 cm^{-1} in the unlabeled sample likely downshifts and overlaps with the positive band at 1518 cm^{-1} seen in both the labeled and unlabeled sample. This indicates that the 1551 (−) and 1537 (+) bands arise from an amide II mode that downshifts upon photoisomerization. This downshift can be interpreted as a weakening of the hydrogen bonding in one or more peptide groups in the protein backbone (*40*). A similar amide II downshift was observed in GPR (*32*) but only at room temperature on an ultrafast time scale. In contrast, in the low-temperature FTIR

difference spectrum of BR, a pair of bands is assigned to the upshift of an amide II mode (*41*).

In the retinal fingerprint region, prominent negative bands are found at 1255, 1234, and 1202 cm^{-1} (Figure 1) close to peaks at 1255, 1234, and 1200 cm^{-1} in GPR (*22*) and 1255 and 1203 cm^{-1} in BR. These bands are also found in the RRS of BPR (*15*) and thus can be assigned unambiguously to retinal vibrations. These negative bands in the BR → K (*20*) difference spectrum have been assigned to various C—C stretching modes of the all-*trans*-retinal chromophore on the basis of comparison to RRS studies of isotopically labeled retinal in BR (*33, 42*). Unlike GPR and light-adapted BR, BPR exhibits a negative band at 1349 cm^{-1} characteristic of contribution from a 13-*cis* photocycle (*31*). This may indicate the presence of some 13-*cis*-retinal in the dark state of BPR. However, in the case of GPR only an all-*trans* chromophore has been detected in the dark (*8*). Similar to GPR, BPR does not exhibit a negative band near 1216 cm^{-1} assigned to the C8−C9 stretching mode in BR (*22, 33*).

Several positive bands appear in the BPR difference spectrum at 1192, 1188, and 1181 cm^{-1}. The 1192 cm^{-1} band is similar to the 1192 cm^{-1} band in GPR (*22*−*24*) and the 1194 cm^{-1} band in BR assigned to the mixed stretching vibration of the 13-*cis*-retinal chromophore (*37, 42*). The 1188 and 1181 cm^{-1} bands possibly result from excitation of a 13-*cis* photocycle as discussed above.

BPR also exhibits a pair of bands at 1015/1008 (−/+) cm^{-1}, most likely due to an upshift in the frequency of methyl rock vibrations seen in RRS at 1012 cm^{-1} (*15*). GPR exhibits a much stronger pair of bands at lower frequency 1007/999 (−/+) cm^{-1} assigned to the methyl rock vibration (*8, 22*). In the hydrogen out-of-plane (HOOP) mode region (900−1000 cm^{-1}) negative/positive bands appear in the BPR → K difference spectrum at 959/967 cm^{-1} similar to the negative/positive bands at 958/966 cm^{-1} in GPR assigned to shift in frequency of a HOOP mode (*22*).

Detection of Protein Vibrations. Peaks in the 1600−1700 cm^{-1} region can arise from the amide I peptide mode of the protein backbone, Schiff base C═N stretching mode of the chromophore, and various amino acid side chain modes such as the C═O stretching mode of Asn and Gln side chains. In the BPR → K difference spectrum peaks of significant intensity appear at 1641 (+), 1665 (−), 1679 (+), 1687 (−), 1690 (−), and 1696 (+) cm^{-1}. The following sections assign these various bands.

(A) Assignment of the Schiff Base C═N Vibration. In order to assign the Schiff base C═N stretching mode in the ground state and K-intermediate of BPR, we utilized H/D exchange, C15D isotope labeling of the chromophore, and total ^{15}N labeling of the protein (Figure 3). Single deuteration at the retinal C15 position downshifts the 1665 cm^{-1} negative band to 1652 cm^{-1} and the positive 1641 cm^{-1} band to 1626 cm^{-1}. Total ^{15}N isotope labeling shifts the 1665 cm^{-1} negative band to 1650 cm^{-1} and the positive 1641 cm^{-1} band to 1624 cm^{-1}. H/D exchange of protein regenerated with unlabeled retinal further downshifts these bands to 1640 and 1626 cm^{-1}, respectively. Finally, H/D exchange of protein reconstituted with singly deuterated retinal at the C15 position downshifts the pair of bands to 1626 and 1601 cm^{-1}. These results show clearly that the C═N stretch frequency of the dark and K-photointermediate states are located at 1665 and 1641 cm^{-1}, respectively. In comparison, the Schiff base C═N

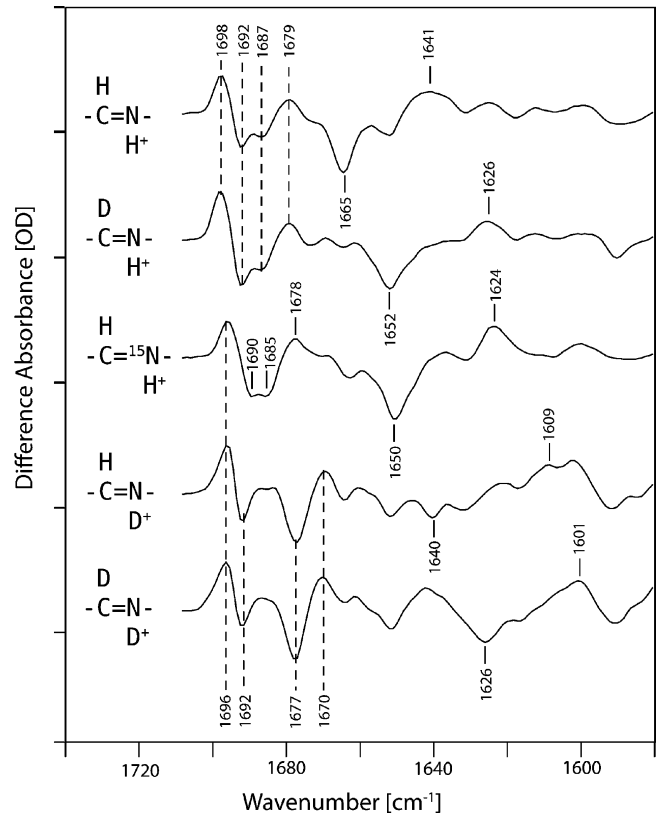

FIGURE 3: FTIR difference spectra recorded at 80 K and 2 cm^{-1} resolution for wild-type BPR containing unlabeled chromophore in H_2O, C15D-labeled chromophore in H_2O, unlabeled chromophore with total ^{15}N-labeled protein, unlabeled chromophore in D_2O, and C15D-labeled chromophore in D_2O. Spacing of *Y*-axis (difference absorbance) markers corresponds to 0.2×10^{-4} OD.

stretch frequencies of the GPR initial state and K-photointermediate are located at 1664 and 1630 cm^{-1}, respectively (*22, 23*). A similar study performed on BR indicates that the C═N vibrations in BR (light adapted) and K occur at 1640 and 1609 cm^{-1}, respectively (*37*). The frequency change in the Schiff base C═N vibration upon H/D exchange correlates with the hydrogen-bonding strength (*43, 44*). In BPR, the downshift in the Schiff base C═N stretching mode induced by H/D exchange is 25 cm^{-1}, in between GPR (29 cm^{-1}) and BR (15 cm^{-1}), indicating that the hydrogen-bonding strength of the Schiff base is weaker in BPR than in GPR but stronger than in BR.

(B) FTIR Difference Spectrum of the Mutant N230S. The BPR → K difference spectrum exhibits a positive band at 1698 cm^{-1} and a negative band at 1692 cm^{-1} which are candidates for the C═O stretching modes of Asn and Gln side chains (*45*). Both BPR and GPR have a polar residue (Asn230 based on the numbering system for GPR sequence) adjacent to Lys231 which forms a covalent Schiff base linkage with all-*trans*-retinal. In contrast, BR has a hydrophobic residue Ala215 adjacent to Lys216, which forms a covalent Schiff base linkage with all-*trans*-retinal. In GPR a pair of bands appearing at 1699/1695 (+/−) cm^{-1} in the GPR → K difference spectrum were assigned to the perturbation of Asn230 on the basis of a GPR N230A mutant (*22*).

In order to see if these bands have a similar origin in BPR the mutant Asn230 → Ser (N230S) was measured (Figure 4). The difference spectra of the N230S mutant and WT are

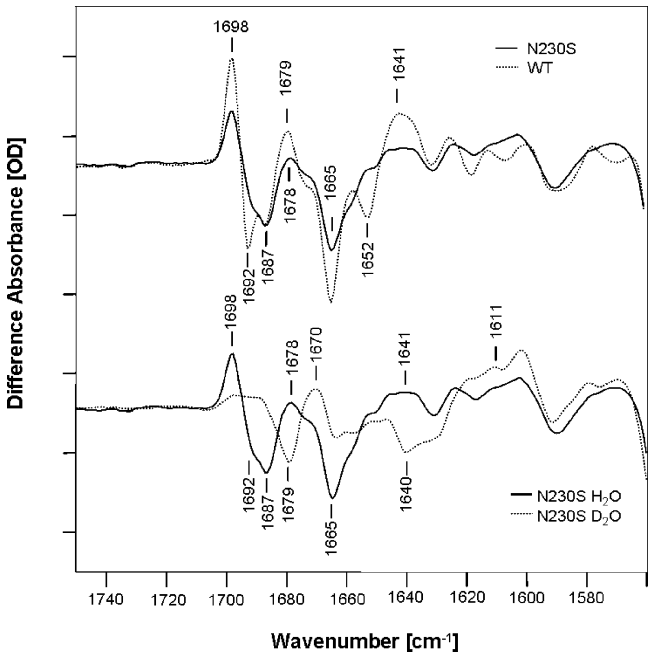

FIGURE 4: Comparison of the WT and N230S BPR difference spectra recorded at 80 K in the 1750−1560 cm^{-1} region in H_2O (top) and comparison of the BPR N230S difference spectra in H_2O and D_2O (bottom). Spacing of *Y*-axis (difference absorbance) markers corresponds to 0.2×10^{-4} OD.

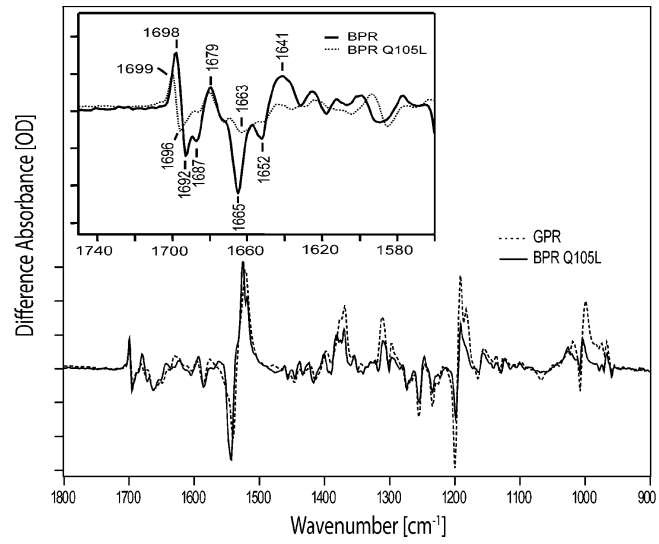

FIGURE 5: Comparison of the WT GPR and Q105L BPR 80 K FTIR difference spectra in the 1800−900 cm^{-1} region. (Inset) Comparison of the wild-type BPR and Q105L BPR 80 K difference spectra in the 1750−1560 cm^{-1} region. Spacing of *Y*-axis (difference absorbance) markers corresponds to 0.2×10^{-4} OD.

very similar below 1560 cm^{-1}, especially in the chromophore ethylenic and fingerprint regions, indicating that the primary photoreaction including all-*trans* to 13-*cis* chromophore isomerization is not significantly affected by the mutation (data not shown). Comparison of wild-type BPR with N230S difference spectra in the 1750−1560 cm^{-1} region (Figure 4) reveals that part of the 1692 cm^{-1} negative band disappears along with part of the intensity of the positive band at 1698 cm^{-1}. This indicates that part of the negative 1692 cm^{-1} band along with part of the positive band at 1698 cm^{-1} arises from perturbation of Asn230 in the BPR primary photoreaction. The increase in frequency indicates that the hydrogen bonding of the Asn230 residue is weaker in the photointermediate (*45*). The remaining intensity at 1698 (+) and 1692 (−) cm^{-1} indicates the presence of a second Asn or Gln group (see below). The N230S mutation also eliminates a negative band at 1652 cm^{-1} and alters the intensity of several other bands in the amide I region. However, it does not appear to affect the frequency of the 1665/1641 (−/+) cm^{-1} bands assigned to the Schiff base in the initial state and photointermediate, indicating the environment and hydrogen bonding of the Schiff base are not altered by this mutation.

Comparison of N230S difference spectra recorded in H_2O vs D_2O reveals the remaining intensity at 1698 (+) and 1692 (−) cm^{-1} in N230S is downshifted by H/D exchange. This result indicates that the unidentified Asn or Gln group giving rise to these peaks undergoes H/D exchange (Figure 4) in contrast to the bands assigned to N230 in the wild-type sample which do not appear to be affected by H/D exchange (see Figure 3, second trace from bottom). This indicates that the Asn230 amide group is not easily accessible for H/D exchange. Note that, as in the WT sample, a similar downshift of the Schiff base vibrations assigned to the initial state and K-intermediate in N230S occurs after H/D exchange, indicating that this mutation does not alter the environment or structure of the Schiff base.

(C) FTIR Difference Spectrum of the Mutant Q105L. As discussed above, the remaining negative intensity at 1692 cm^{-1} and positive intensity at 1698 cm^{-1} may arise from a second Asn or Gln group in BPR which undergoes an alteration during the primary photoreaction. One candidate is Gln105 which in GPR is a Leu. Previously, it was shown that a BPR Q105L mutation switches the visible absorption phenotype of BPR to that of GPR (*11*−*13, 46*). Such an assignment is strongly supported by the similarity of the low-temperature FTIR difference spectra of the Q105L mutant and GPR (Figure 5). In this mutant part of the intensity at 1692 and 1698 cm^{-1} disappears, leaving bands at 1699 (+) and 1692 (−) cm^{-1} which are attributed to the residue Asn230 in the mutant Q105L (Figure 5, inset). Therefore, the large bands at 1698/1692 (+/−) in the WT are due to perturbation of both Asn230 and Gln105. The bands at 1665 (−) and 1641 (+) cm^{-1} assigned to the C=N Schiff base vibrations of the dark state and K-intermediate are also affected, indicating that Gln105 in BPR interacts with the Schiff base in both states.

(D) Identification of Bands Due to Internal Water Molecules. A single negative band at 3642 cm^{-1} is observed in the 3500−3700 cm^{-1} region of the BPR → K difference spectrum (Figure 6). Bands in this region typically arise from the O−H stretching vibrations of weakly hydrogen-bonded protein side-chain hydroxyl groups or internal water molecules. In GPR, three bands at 3628 (−), 3620 (+), and 3542 (+) cm^{-1} were assigned to internal water molecules (*22, 24*). The negative peak at 3642 cm^{-1} in BPR is identical in frequency to the 3642 cm^{-1} negative peak in the BR → K spectrum (*47, 48*). However, unlike BR there is no positive band detected within the signal/noise. $H_2{}^{18}O$ exchange in BPR downshifts the 3542 cm^{-1} band 12 cm^{-1} to 3630 cm^{-1}, consistent with a $^{16}O \rightarrow {}^{18}O$ isotope shift, confirming that this band is due to an internal water molecule.

The Asn230 → Ser mutant exhibits the same negative band at 3642 cm^{-1}, indicating that this corresponding water

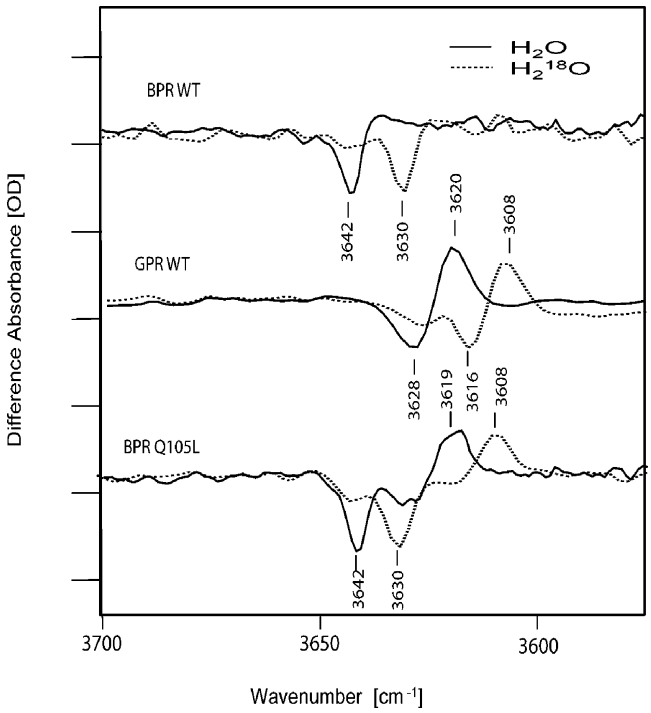

FIGURE 6: Comparison of the WT BPR, WT GPR, and Q105L BPR 80 K FTIR difference spectra in the 3700−3550 cm^{-1} region: (top) WT BPR in H_2O (solid line) and $H_2{}^{18}O$ (dotted line); (middle) WT GPR in H_2O (solid line) and $H_2{}^{18}O$ (dotted line); (bottom) Q105L BPR in H_2O (solid line) and $H_2{}^{18}O$ (dotted line). Spacing of *Y*-axis (difference absorbance) markers corresponds to 0.1×10^{-4} OD.

molecule does not closely interact with Asn230 (data not shown). The Q105L mutation (Figure 6, lower trace) also leaves this band unaltered but introduces a second water molecule which is very similar to the one previously identified in GPR (*22*). This is indicated by a negative band near 3628 cm^{-1} and positive band at 3620 cm^{-1} seen also in the GPR difference spectra. In addition, all of these bands downshift as expected in $H_2{}^{18}O$ based on results from the WT BPR and GPR spectra (see Figure 6). Thus, the BPR Q105L mutation appears to allow a second water molecule to enter into the active site of BPR in a position that is almost identical in environment and behavior to the water molecule detected in GPR. Furthermore, the GPR L105Q mutation does not disturb the structure or structural changes of the first water molecule in BPR. As discussed below an attractive explanation for the appearance of this second water molecule is that it forms a hydrogen bond with the Schiff base instead of with Gln105 which is now replaced by the hydrophobic leucine residue.

DISCUSSION AND CONCLUSIONS

The current study focuses on elucidating the molecular events which occur in the primary photoreaction of BPR and contrasting them with GPR, the two major subgroups of proteorhodopsins. Several conclusions can be deduced:

(1) Similar to GPR, the retinal chromophore undergoes all-*trans* to 13-*cis* photoisomerization upon photon absorption. Furthermore, the structure of the BPR chromophore in the dark state (prior to photoexcitation) is very similar to the GPR chromophore since the frequencies of negative bands in the chromophore fingerprint region are very similar. This conclusion is also supported by RRS measurements

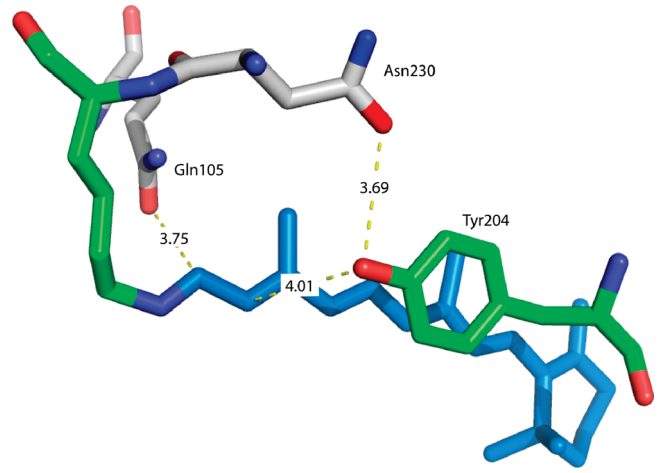

FIGURE 7: Hypothesized positions of residues Gln105, Asn230, and Tyr204 relative to the retinal chromophore and protonated Schiff base. The figure was created using PyMol software (DeLano, W. L. (2003) DeLano Scientific LLC, South San Francisco, CA 94080) from the PDB file 1JGJ by substituting the specific BPR residues shown onto the SRII crystal structure based on recent findings (*54*) as discussed in the text. The BPR residues were imported to minimize steric interactions with the surrounding residues only. This model is only presented to provide a possible pathway and does not represent the free energy minima of the protein.

made on BPR and GPR (*15*). A similar conclusion can be reached about the structure of the K chromophore based on the similarity of positive bands in the GPR and BPR primary photoreaction difference spectrum. The only exceptions are the presence of a positive feature at 1188 cm^{-1} and a negative band at 1348 cm^{-1} which are not present in GPR and may reflect the product of a 13-*cis* form of BPR which has previously been reported in BR (*31*).

(2) Despite the similar Schiff base stretch frequency of BPR and GPR in the dark-adapted state, its hydrogen-bonding strength appears to be different based on the different H/D exchange induced downshifts observed. Such differences are also confirmed by RRS measurements (*15*) and most likely reflect an altered environment of the Schiff base due to the substitution of Glu105 in BPR for Leu105 in GPR (see point 5 below).

(3) Similar to GPR, the residue Asn230 undergoes a weakening in hydrogen bonding during the BPR primary photoreaction as indicated by bands at 1698/1692 (+/−) cm^{-1} assigned in part to the side-chain C═O stretching mode of Asn230 on the basis of the mutant N230S. Since this substitution does not alter the Schiff base frequency or the H/D-induced downshift of the Schiff base frequency, we conclude it does not directly interact with the Schiff base. Furthermore, Asn230 is buried in the protein interior and not accessible to bulk solvent since the Asn vibrations do not undergo an H/D-induced downshift in D_2O. A possible explanation for these observations is that Asn230 forms a strong hydrogen bond with Tyr204, which is located nearby on the basis of the X-ray structure of sensory rhodopsin II. Changes in the hydrogen bonding of Asn230 could then be in response to a change in the position of Tyr204 due to chromophore isomerization since it is located adjacent to the retinal polyene chain near C12−13 (Figure 7). In this case we would expect bands due to Tyr204 to also appear in the difference spectrum. Although it is not possible to assign tyrosine vibrations unambiguously to bands in the difference

spectrum without use of mutagenesis or isotope labeling, bands near 1260−1270 cm^{-1} in the region of tyrosine (*49*) do appear and are perturbed in the N230S and Q105L mutant (data not shown). Previously, bands in this region of the BR to K difference spectrum of bacteriorhodopsin have been assigned to the homologous residue Tyr185 (*50*).

(4) Gln105 also undergoes a weakening of its hydrogen bonding during the BPR primary photoreaction. However, in contrast to Asn230, Gln 105 is accessible for H/D exchange as evidenced by the disappearance of the 1698 (+) and 1692 (−) cm^{-1} bands in the N230S D2O spectrum (Figure 4). In addition, substitution of Gln with Leu perturbs the Schiff base C=N stretch frequency and hydrogen bond strength. On this basis, and by comparison with X-ray derived structures for other microbial rhodopsins (see below), we conclude that Gln105 likely interacts with the C=N Schiff base and responds to movement of this group due to chromophore isomerization during the formation of the K photoproduct. One interesting possibility is that reprotonation of the Schiff base later in the BPR photocycle during formation of the N intermediate occurs through a proton wire involving Gln105.

(5) Perturbation of a water molecule is detected in the primary transition of both BPR (this paper) and GPR (*22*−*24*). Although the frequency of OH stretch mode of this water is different in BPR (3642 cm^{-1}) and GPR (3628 cm^{-1}), it might be assumed both reflect the same water but in a slightly different environment. However, our results show that both waters exist in the BPR mutant Q105L as indicated by the appearance of *both bands*.

As discussed below, this may indicate that the appearance of the GPR-like water (band at 3628 cm^{-1}) in BPR is due to a vacancy left by removal of the hydrogen-bonding glutamine group and replacement with the hydrophobic leucine. It is also interesting to note that the water found in BPR with a frequency of 3642 cm^{-1} is identical to the OH stretch frequency of a water molecule detected in bacteriorhodopsin (BR) and assigned previously to W401 located in the X-ray-derived BR structure as part of a pentagonal water cluster connected to the Schiff base and two negative counterions Asp85 and Asp212 (*51, 52*). Importantly, in the case of BR recent time-resolved FTIR studies indicate that these water molecules are involved in the proton transfer process (*53*). Unlike liquid waters, the precise arrangement of specific waters in BR appears to facilitate a controlled Grotthuss proton transfer reaction. If a similar water molecule exists in BPR, its absence in GPR based on the disappearance of this band might account for differences in several of the properties of GPR and BPR including its proton pumping properties, photocycle, and visible absorption maximum. It will be important in the future studies to further elucidate the role of these waters in proteorhodopsins and contrast to BR in order to see if the overall proton pump mechanism is the same in the two proteins.

(6) Although high-resolution structures of GPR or BPR have not yet been elucidated, the above results can be partially understood on the basis of previously solved crystallographic structural models for the microbial rhodopsins BR and SRII. In accordance with recent findings (*17*) that the absorption properties of BPR at high pH are much better modeled by sensory rhodopsin II (SRII), we use the sensory rhodopsin II structure (*54*) as the basis for homology modeling of BPR (as shown in Figure 7). Here we have made appropriate substitutions of key residues including Asn230 for Thr204 and Gln105 for Ile83. However, we have not altered the position of the Schiff base counterions (Asp75). Note that the BPR residues were imported to minimize steric interactions with the surrounding residues only. This model is only presented to provide a possible structure of BPR based on SRII and does not represent the free energy minima of the protein.

(7) As seen in Figure 7, Gln 105 is in a position to interact directly with the Schiff base, thereby accounting for the appearance of bands assigned to BPR in the primary phototransition. Due to the interaction of Gln105 with the Schiff base it is likely it also plays a role in the opsin shift of BPR (*55, 56*) similar to the interaction of Thr89 in bacteriorhodopsin (*57*). In agreement, recently an energy minimization of the BPR structure predicted a hydrogen bond between Gln105 and the hydrogen of carbon 15 on the retinal chain; the Schiff base carbon atom and Gln105 plays an important role in the color tuning of BPR (*17*). Such an interaction could explain why the replacement of Gln105 with Leu in GPR as well as in the BPR mutant Q105L (*14*) results in the 30 nm red shift of its λ_{max} compared to that of BPR.

ACKNOWLEDGMENT

We thank Dr. Weiwu Wang for assistance with plasmid constructions and Dr. Jerzy Olejnik for synthesis of the C15D retinal.

REFERENCES

1. Beja, O., Aravind, L., Koonin, E. V., Suzuki, M. T., Hadd, A., Nguyen, L. P., Jovanovich, S. B., Gates, C. M., Feldman, R. A., Spudich, J. L., Spudich, E. N., and DeLong, E. F. (2000) Bacterial rhodopsin: evidence for a new type of phototrophy in the sea. *Science 289*, 1902–1906.
2. Rusch, D. B., Halpern, A. L., Sutton, G., Heidelberg, K. B., Williamson, S., Yooseph, S., Wu, D., Eisen, J. A., Hoffman, J. M., Remington, K., Beeson, K., Tran, B., Smith, H., Baden-Tillson, H., Stewart, C., Thorpe, J., Freeman, J., rews-Pfannkoch, C., Venter, J. E., Li, K., Kravitz, S., Heidelberg, J. F., Utterback, T., Rogers, Y.-H., Falc, n, L. I., Souza, V., Bonilla-Rosso, G., Eguiarte, L. E., Karl, D. M., Sathyendranath, S., Platt, T., Bermingham, E., Gallardo, V., Tamayo-Castillo, G., Ferrari, M. R., Strausberg, R. L., Nealson, K., Friedman, R., Frazier, M., and Venter, J. C. (2007) The Sorcerer II Global Ocean Sampling Expedition: Northwest Atlantic through Eastern Tropical Pacific. *PLoS Biol. 5*, e77.
3. Spudich, J. L., and Jung, K.-H. (2005) Microbial Rhodopsins: Phylogenetic and Functional Diversity, in *Handbook of Photosensory Receptors* (Briggs, W., and Spudich, J. L., Eds.) pp 1–24, Wiley-VCH, New York.
4. Venter, J. C., Remington, K., Heidelberg, J. F., Halpern, A. L., Rusch, D., Eisen, J. A., Wu, D., Paulsen, I., Nelson, K. E., Nelson, W., Fouts, D. E., Levy, S., Knap, A. H., Lomas, M. W., Nealson, K., White, O., Peterson, J., Hoffman, J., Parsons, R., Baden-Tillson, H., Pfannkoch, C., Rogers, Y. H., and Smith, H. O. (2004) Environmental genome shotgun sequencing of the Sargasso Sea. *Science 304*, 66–74.
5. Sabehi, G., Loy, A., Jung, K. H., Partha, R., Spudich, J. L., Isaacson, T., Hirschberg, J., Wagner, M., and Beja, O. (2005) New insights into metabolic properties of marine bacteria encoding proteorhodopsins. *PLoS Biol. 3*, e273.
6. Beja, O., Spudich, E. N., Spudich, J. L., Leclerc, M., and DeLong, E. F. (2001) Proteorhodopsin phototrophy in the ocean. *Nature 411*, 786–789.
7. Friedrich, T., Geibel, S., Kalmbach, R., Chizhov, I., Ataka, K., Heberle, J., Engelhard, M., and Bamberg, E. (2002) Proteorhodopsin is a light-driven proton pump with variable vectoriality. *J. Mol. Biol. 321*, 821–838.

8. Dioumaev, A. K., Brown, L. S., Shih, J., Spudich, E. N., Spudich, J. L., and Lanyi, J. K. (2002) Proton transfers in the photochemical reaction cycle of proteorhodopsin. *Biochemistry 41*, 5348–5358.
9. Krebs, R. A., DeVita, A. M., Parthasarathy, R., Alexiev, U., Dunmire, D., and Braiman, M. S. (2002) Purification and spectroscopic studies of proteorhodopsin. *Biophys. J. 82*, 224A–224A.
10. Bielawski, J. P., Dunn, K. A., Sabehi, G., and Beja, O. (2004) Darwinian adaptation of proteorhodopsin to different light intensities in the marine environment. *Proc. Natl. Acad. Sci. U.S.A. 101*, 14824–14829.
11. Kelemen, B. R., Du, M., and Jensen, R. B. (2003) Proteorhodopsin in living color: diversity of spectral properties within living bacterial cells. *Biochim. Biophys. Acta 1618*, 25–32.
12. Man, D., Wang, W., Sabehi, G., Aravind, L., Post, A. F., Massana, R., Spudich, E. N., Spudich, J. L., and Beja, O. (2003) Diversification and spectral tuning in marine proteorhodopsins. *EMBO J. 22*, 1725–1731.
13. Man-Aharonovich, D., Sabehi, G., Sineshchekov, O. A., Spudich, E. N., Spudich, J. L., and Beja, O. (2004) Characterization of RS29, a blue-green proteorhodopsin variant from the Red Sea. *Photochem. Photobiol. Sci. 3*, 459–462.
14. Wang, W. W., Sineshchekov, O. A., Spudich, E. N., and Spudich, J. L. (2003) Spectroscopic and photochemical characterization of a deep ocean proteorhodopsin. *J. Biol. Chem. 278*, 33985–33991.
15. Kralj, J. M., Spudich, E. N., Spudich, J. L., and Rothschild, K. J. (2008) Raman spectroscopy reveals direct chromophore interactions in the Leu/Gln 105 spectral tuning switch of proteorhodopsins. *J. Phys. Chem. B 112*, 11770–11776.
16. Kralj, J. M., Bergo, V. B., Amsden, J. J., Spudich, E. N., Spudich, J. L., and Rothschild, K. J. (2008) Protonation state of Glu142 differs in the green- and blue-absorbing variants of proteorhodopsin. *Biochemistry 47*, 3447–3453.
17. Hillebrecht, J. R., Galan, J., Rangarajan, R., Ramos, L., McCleary, K., Ward, D. E., Stuart, J. A., and Birge, R. R. (2006) Structure, function, and wavelength selection in blue-absorbing proteorhodopsin. *Biochemistry 45*, 1579–1590.
18. Braiman, M. S., Ahl, P. L., and Rothschild, K. J. (1987) Millisecond Fourier-transform infrared difference spectra of bacteriorhodopsin's M412 photoproduct. *Proc. Natl. Acad. Sci. U.S.A. 84*, 5221–5225.
19. Rothschild, K., and Marrero, H. (1982) Infrared evidence that the Schiff base of bacteriorhodopsin is protonated: bR570 and K intermediates. *Proc. Natl. Acad. Sci. U.S.A. 79*, 4045–4049.
20. Rothschild, K. J., Roepe, P., Lugtenburg, J., and Pardoen, J. A. (1984) Fourier transform infrared evidence for Schiff base alteration in the first step of the bacteriorhodopsin photocycle. *Biochemistry 23*, 6103–6109.
21. Rothschild, K. J., Zagaeski, M., and Cantore, W. A. (1981) Conformational changes of bacteriorhodopsin detected by Fourier transform infrared difference spectroscopy. *Biochem. Biophys. Res. Commun. 103*, 483–489.
22. Bergo, V., Amsden, J. J., Spudich, E. N., Spudich, J. L., and Rothschild, K. J. (2004) Structural changes in the photoactive site of proteorhodopsin during the primary photoreaction. *Biochemistry 43*, 9075–9083.
23. Furutani, Y., Ikeda, D., Shibata, M., and Kandori, H. (2006) Strongly hydrogen-bonded water molecule is observed only in the alkaline form of proteorhodopsin. *Chem. Phys. 324*, 705–708.
24. Ikeda, D., Furutani, Y., and Kandori, H. (2007) FTIR study of the retinal Schiff base and internal water molecules of proteorhodopsin. *Biochemistry 46*, 5365–5373.
25. Imasheva, E. S., Balashov, S. P., Wang, J. M., Dioumaev, A. K., and Lanyi, J. K. (2004) Selectivity of retinal photoisomerization in proteorhodopsin is controlled by aspartic acid 227. *Biochemistry 43*, 1648–1655.
26. Xiao, Y., Partha, R., Krebs, R., and Braiman, M. (2005) Time-resolved FTIR spectroscopy of the photointermediates involved in fast transient H^+ release by proteorhodopsin. *J. Phys. Chem. 109*, 634–641.
27. Bergo, V., Spudich, E. N., Spudich, J. L., and Rothschild, K. J. (2002) A Fourier transform infrared study of Neurospora rhodopsin: similarities with archaeal rhodopsins. *Photochem. Photobiol. 76*, 341–349.
28. Kandori, H., Shimono, K., Sudo, Y., Iwamoto, M., Shichida, Y., and Kamo, N. (2001) Structural changes of pharaonis phoborhodopsin upon photoisomerization of the retinal chromophore: infrared spectral comparison with bacteriorhodopsin. *Biochemistry 40*, 9238–9246.
29. Siebert, F., and Mantele, W. (1983) Investigation of the primary photochemistry of bacteriorhodopsin by low-temperature Fourier-transform infrared spectroscopy. *Eur. J. Biochem./FEBS 130*, 565–573.
30. DeGrip, W. J., and Rothschild, K. J. (2000) Structure and Mechanism of Vertebrate Visual Pigments, in *Molecular Mechanisms in Visual Transduction* (Stravenga, D. G., de Grip, W. J., and Pugh, E. N., Eds.) pp 1−54, Elsevier Science B.V., Amsterdam.
31. Roepe, P. D., Ahl, P. L., Herzfeld, J., Lugtenburg, J., and Rothschild, K. J. (1988) Tyrosine protonation changes in bacteriorhodopsin. A Fourier transform infrared study of bR548 and its primary photoproduct. *J. Biol. Chem. 263*, 5110–5117.
32. Amsden, J. J., Kralj, J. M., Chieffo, L. R., Wang, X., Erramilli, S., Spudich, E. N., Spudich, J. L., Ziegler, L. D., and Rothschild, K. J. (2007) Subpicosecond protein backbone changes detected during the green-absorbing proteorhodopsin primary photoreaction. *J. Phys. Chem. 111*, 11824–11831.
33. Smith, S. O., Braiman, M. S., Myers, A. B., Pardoen, J. A., Courtin, J. M. L., Winkel, C., Lugtenburg, J., and Mathies, R. A. (1987) Vibrational analysis of the all-trans-retinal chromophore in light-adapted bacteriorhodopsin. *J. Am. Chem. Soc. 109*, 3108–3125.
34. Bernard, M. T., MacDonald, G. M., Nguyen, A. P., Debus, R. J., and Barry, B. A. (1995) A difference infrared study of hydrogen bonding to the Z tyrosyl radical of photosystem II. *J. Biol. Chem. 270*, 1589–1594.
35. Wang, R., Sivakumar, V., Johnson, T. W., and Hastings, G. (2004) FTIR difference spectroscopy in combination with isotope labeling for identification of the carbonyl modes of P700 and $P700^+$ in photosystem I. *Biophys. J. 86*, 1061–1073.
36. Bagley, K., Dollinger, G., Eisenstein, L., Singh, A. K., and Zimanyi, L. (1982) Fourier transform infrared difference spectroscopy of bacteriorhodopsin and its photoproducts. *Proc. Natl. Acad. Sci. U.S.A. 79*, 4972–4976.
37. Rothschild, K. J., Marrero, H., Braiman, M., and Mathies, R. (1984) Primary photochemistry of bacteriorhodopsin: comparison of Fourier transform infrared difference spectra with resonance Raman spectra. *Photochem. Photobiol. 40*, 675–679.
38. Aton, B., Doukas, A. G., Callender, R. H., Becher, B., and Ebrey, T. G. (1977) Resonance Raman studies of the purple membrane. *Biochemistry 16*, 2995–2999.
39. Bergo, V., Spudich, E. N., Spudich, J. L., and Rothschild, K. J. (2003) Conformational changes detected in a sensory rhodopsin II-transducer complex. *J. Biol. Chem. 278*, 36556–36562.
40. Bellamy, L. J. (1968) *The Infrared Spectra of Complex Molecules*, Vol. 2, Chapman and Hall, London.
41. Kluge, T., Olejnik, J., Smilowitz, L., and Rothschild, K. J. (1998) Conformational changes in the core structure of bacteriorhodopsin. *Biochemistry 37*, 10279–10285.
42. Smith, S. O., Pardoen, J. A., Lugtenburg, J., and Mathies, R. A. (1987) Vibrational analysis of the 13-cis-retinal chromophore in dark-adapted bacteriorhodopsin. *J. Phys. Chem. 91*, 804–819.
43. Baasov, T., Friedman, N., and Sheves, M. (1987) Factors affecting the C═N stretching in protonated retinal Schiff base: a model study for bacteriorhodopsin and visual pigments. *Biochemistry 26*, 3210–3217.
44. Gilson, H. S. R., Honig, B. H., Croteau, A., Zarrilli, G., and Nakanishi, K. (1988) Analysis of the factors that influence the carbon:nitrogen stretching frequency of polyene Schiff bases. Implications for bacteriorhodopsin and rhodopsin. *Biophys. J. 53*, 261–269.
45. Barth, A. (2000) The infrared absorption of amino acid side chains. *Prog. Biophys. Mol. Biol. 74*, 141–173.
46. Jung, K.-H., Trivedi, V. D., and Spudich, J. L. (2003) Demonstration of a sensory rhodopsin in eubacteria. *Mol. Microbiol. 47*, 1513–1522.
47. Fischer, W., Sonar, S., Marti, T., Khorana, H. G., and Rothschild, K. J. (1994) Detection of a water molecule in the active site of bacteriorhodopsin: Hydrogen bonding changes during the primary photoreaction. *Biochemistry 33*, 12757–12762.
48. Maeda, A., Sasaki, J., Shichida, Y., and Yoshizawa, T. (1992) Water structural changes in the bacteriorhodopsin photocycle: Analysis by Fourier transform infrared spectroscopy. *Biochemistry 31*, 462–467.
49. Rothschild, K. J., Roepe, P., Ahl, P. L., Earnest, T. N., Bogomolni, R. A., Das Gupta, S. K., Mulliken, C. M., and Herzfeld, J. (1986) Evidence for a tyrosine protonation change during the primary

phototransition of bacteriorhodopsin at low temperature. *Proc. Natl. Acad. Sci. U.S.A. 83*, 347–351.
50. Braiman, M. S., Mogi, T., Marti, T., Stern, L. J., Khorana, H. G., and Rothschild, K. J. (1988) Vibrational spectroscopy of bacteriorhodopsin mutants: light-driven proton transport involves protonation changes of aspartic acid residues 85, 96, and 212. *Biochemistry 27*, 8516–8520.
51. Neutze, R., Pebay-Peyroula, E., Edman, K., Royant, A., Navarro, J., and Landau, E. M. (2002) Bacteriorhodopsin: a high-resolution structural view of vectorial proton transport. *Biochim. Biophys. Acta 1565*, 144–167.
52. Shibata, M., and Kandori, H. (2005) FTIR studies of internal water molecules in the Schiff base region of bacteriorhodopsin. *Biochemistry 44*, 7406–7413.
53. Garczarek, F., and Gerwert, K. (2006) Functional waters in intraprotein proton transfer monitored by FTIR difference spectroscopy. *Nature 439*, 109–112.
54. Luecke, H., Schobert, B., Lanyi, J. K., Spudich, E. N., and Spudich, J. L. (2001) Crystal structure of sensory rhodopsin II at 2.4 angstroms: insights into color tuning and transducer interaction. *Science 293*, 1499–1503.
55. Lugtenburg, J., Muradin-Szweykowska, M., Heeremans, C., and Pardoen, J. A. (1986) Mechanism for the opsin shift of retinal's absorption in bacteriorhodopsin. *J. Am. Chem. Soc. 108*, 3104–3105.
56. Spudich, J. L., McCain, D. A., Nakanishi, K., Okabe, M., Shimizu, N., Rodman, H., Honig, B., and Bogomolni, R. A. (1986) Chromophore/protein interaction in bacterial sensory rhodopsin and bacteriorhodopsin. *Biophys. J. 49*, 479–483.
57. Russell, T. S., Coleman, M., Rath, P., Nilsson, A., and Rothschild, K. J. (1997) Threonine-89 participates in the active site of bacteriorhodopsin: evidence for a role in color regulation and Schiff base proton transfer. *Biochemistry 36*, 7490–7497.

BI800945T